MARK A. BAKER, STEPHEN A. MACK, and HOWARD C. SCHOEBERLEIN

STATISTICAL ASPECTS OF TURBULENCE AND MICROSTRUCTURE IN THE OCEAN

The ocean has a large range of length scales controlled by vastly different physical processes. Patches of small-scale fluctuations in velocity (turbulence) and temperature and salinity (microstructure) are distributed intermittently in time and space throughout the ocean. This article discusses the sources and statistics of small-scale fluctuations along with techniques to discriminate between sources of microstructure in the ocean.

INTRODUCTION

The ocean has complex velocity and scalar fields with a staggeringly wide spectrum of dynamically important length scales ranging from the mesoscale 1000-km scales of ocean circulation patterns down to the millimeter scales of small-scale turbulence. The smaller-scale end of the spectrum, represented by scales on the order of 10 m down to centimeters, is the subject of this article. Determining sources of small-scale fluctuations in velocity (turbulence) and temperature, conductivity, and salinity (microstructure) and the relative contributions of each source to vertical diffusion is a very active field of research in oceanography. An understanding of the distribution and sources of turbulence and microstructure has been a focus of analysis of at-sea microstructure measurements gathered by The Johns Hopkins University Applied Physics Laboratory for over a decade.

Small-scale velocity fluctuations act on the background gradients of scalar quantities such as temperature, conductivity, and salinity to produce microstructure. Double-diffusive convection, a consequence of the large difference in the molecular diffusion rates of temperature and salt, also produces microstructure, but in a manner fundamentally different from turbulence. Salt fingers, a form of double-diffusive convection, vertically transport (diffuse) greater amounts of salt and nitrates than heat, whereas turbulence vertically transports (diffuses) salt, nitrates, and heat at the same rate. The temperature and salinity gradients observed in the upper portion of the large midlatitude Central Water masses of the ocean indicate that these are likely areas for double-diffusive convection.[1] The microstructure patches also contain fluctuations of nitrates, oxygen, or any other scalar property with a vertical gradient that is mixed by the turbulence or affected by salt fingering. The rates at which these other scalar properties are diffused vertically by turbulence and salt fingering can be directly tied to the vertical diffusion rates of temperature and salinity. Within an oceanic control volume, estimation of the average microstructure activity allows estimation of the average vertical diffusion rates of temperature and salinity. The intermittency of microstructure activity within a given oceanic control volume presents a difficult sampling problem.

An understanding of the vertical diffusion rates of scalar properties such as heat, salt, and inorganic nitrogen is important for planetary-wide issues such as global warming, climate, and large-scale ocean circulation models. The increase in carbon dioxide in the Earth's atmosphere has led to predictions of global warming, since increasing levels of carbon dioxide cause the atmosphere to retain increasing amounts of the heat radiated from the Earth. Climate is largely determined by the complex interactions between the atmosphere and the ocean. The major solar input of heat into the Earth's climatic system occurs at the equator. Both the atmosphere and the ocean transport heat from the equatorial regions toward the poles. The ocean has a much greater heat capacity than the atmosphere, but the ocean circulation moves toward the poles much more slowly than the atmospheric circulation. Correct modeling of the ocean circulation leads to a better understanding of the dynamics of our climatic system.

The ocean is considered, by modelers of the Earth's carbon cycle, to be the major sink for atmospheric carbon dioxide.[2] The rate at which the ocean can absorb carbon dioxide is proportional to the rate that photosynthesis by photosynthetic microorganisms can utilize inorganic carbon. Some of the inorganic carbon incorporated by the microorganisms is removed from the cycle by sinking and vertical transport losses to deep water. The rate of photosynthesis in the ocean is limited by the rate at which inorganic nitrogen is supplied from deep ocean waters to the microorganisms in the illuminated upper ocean. Models of the inorganic carbon–nitrogen cycle have neglected the effects of salt fingering and have generally assumed that the supply of inorganic nitrogen to the upper

ocean is controlled by turbulence. But vertical diffusion rates of salt[3] and inorganic nitrogen due to salt fingers may be 10 times greater than those due to turbulence. Changes in weather and precipitation patterns due to global warming could affect the vertical temperature and salinity gradients in the ocean in a way that leads to an increase in salt fingering activity. In that case, salt fingering could provide a mechanism to counteract increased global warming through the positive effect of salt fingering on the rate of photosynthesis in the upper ocean.[2]

Measurements of turbulence and microstructure in the ocean have been gathered for over two decades, but the inherent variability in ocean environments and the slowly varying (in space and time) large-scale random processes that are the sources of small-scale activity still leave the ocean woefully undersampled, both in space and time. In addition, small-scale activity is intermittent in time and space, presenting challenging sampling and statistical problems. Vertical profiles allow easier access to the physics underlying a particular patch of small-scale activity, but provide little information on the horizontal extent. Sample sets that cover a large horizontal extent are difficult to obtain by the vertical profiling approach. A towed chain, with a reasonable vertical aperture of thermistor and conductivity sensors, generates a two-dimensional slice of the ocean and quickly provides a large microstructure sample set. Large data sets obtained by towed chains of thermistors and conductivity sensors only partially address the sampling and source issues. Ideally, small-scale velocity, temperature, and conductivity measurements should be coupled with colocated velocity and shear measurements over the larger vertical scales appropriate to the physical mechanism generating the turbulence and microstructure activity. The identification of the sources of turbulence and microstructure would then be less difficult.

In this article we will discuss background information on the ocean environment relevant to understanding small-scale mixing processes along with the sources of small-scale activity. The statistics of turbulence and microstructure and techniques to distinguish between sources of microstructure are also presented.

THE OCEAN ENVIRONMENT

The ocean is a stratified medium that typically increases in density with increasing depth. The density of seawater ρ (a nominal value is 1.025 gm/cm^3) at a particular depth is largely determined by temperature (T) and salinity (S). The relative contributions to density by temperature and salinity are defined by the coefficients of thermal expansion, $\alpha = -(1/\rho)(\partial\rho/\partial T)$ (salinity and pressure held constant) and haline contraction, $\beta = (1/\rho)(\partial\rho/\partial S)$ (temperature and pressure held constant). Depth or pressure also plays a role since seawater is compressible; therefore, increasing depth implies increased density. The role of pressure in determining the density of seawater is largely constrained to the deep ocean. The temperature and salinity field of the ocean is complex; water masses with different temperature and salinity characteristics interact throughout the ocean. The velocity field of the ocean is also complex; large-scale circulation patterns, currents, surface waves, internal waves, and near inertial frequency internal waves are only some of the large-scale processes that affect small-scale mixing activity in the ocean. Fronts, which are identified by sharp temperature, salinity, and density changes occurring over a few kilometers, are another source of small-scale activity. This complex system of currents, water masses, and physical processes poses a difficult sampling problem for investigators seeking to parameterize small-scale mixing activity in the ocean. Researchers have generally focused on only a small aspect of these physical processes and then only in a few areas of the ocean. The Laboratory's at-sea experiments have largely focused on the upper 200 m of the Sargasso Sea (western portion of the North Atlantic Ocean) and the Tongue of the Ocean (near the Bahamas).

We can divide the upper ocean vertically into three regimes: a well-mixed surface layer; the seasonal pycnocline, where the density changes sharply over a few tens of meters; and the main pycnocline, where the density increases slowly with depth. Figure 1 shows the three regimes from the average of several vertical profiles

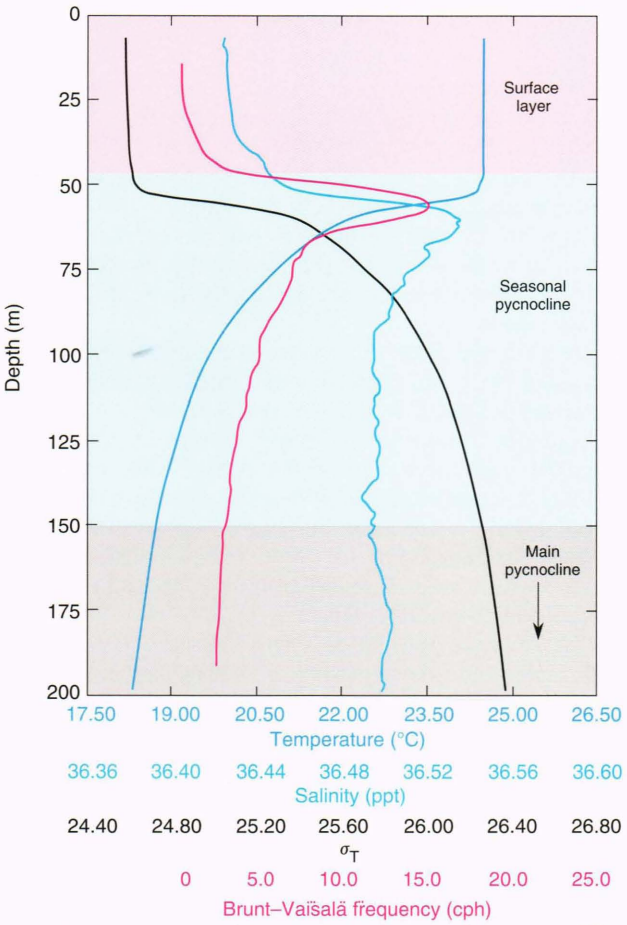

Figure 1. Vertical profiles of temperature, salinity, $\sigma_T = 1000(\rho - 1)$, and the Brunt–Väisälä frequency (see Sources of Microstructure section) based on the average of ten vertical profiles from the Sargasso Sea. The depth regimes corresponding to the surface layer, seasonal pycnocline, and the beginning of the main pycnocline are indicated. Temperature and salinity both decrease over the depth range of 60 to 100 m, pointing toward salt fingering as a potential source of microstructure.

typical of the Sargasso Sea. Between 60 and 100 m, both temperature and salinity decrease with depth, but density increases with depth because of the significantly greater contribution of temperature to the density. Since the profile only extends to a depth of about 200 m, only the beginning of the main pycnocline is shown.

The surface layer falls into three modes: active mixing, mixed, and stratified. The first two are marked by only small changes in density over the depth of the surface layer. The mixed mode implies that mixing activity has ceased (dampened by, for example, surface heating due to solar input), but only small changes in density are observed with increasing depth within the surface layer. The stratified mode occurs when the upper portion of the water column exhibits significant stratification right to the surface. This typically occurs under the conditions of low wind coupled with surface heating. Activity in the surface layer is generally controlled by wind and solar forcing; frontal regions between water masses of different types also produce small-scale activity in the surface layer. Active mixing in the surface layer typically is caused by either high winds coupling into the surface layer through wind–wave interactions or by convection induced by surface cooling. Diurnal change in solar heating may sometimes play a larger role in the dynamics of the upper layer than mixing produced by wind forcing. Nighttime cooling of the near surface water, even without wind, can lead to strong mixing through vertical convection. The surface water becomes more dense than the water below and becomes hydrodynamically unstable. Solar heating in the afternoon can suppress wind-driven mixing in the surface layer by increasing the density gradient to the point that the surface forcing due to the wind cannot overcome the buoyancy force due to the stratification.

An example of the importance of the diurnal cycle was revealed by vertical profiles of turbulence and microstructure obtained during an APL field test in January 1982 in the Tongue of the Ocean. Mixing in the surface layer strongly depended on the diurnal solar cycle.[4] A well-mixed surface layer with strong mixing activity extending to the seasonal pycnocline occurred at night because of convective mixing induced by surface cooling. Daytime solar heating strongly suppressed mixing activity in the surface layer.

The seasonal pycnocline is a transitional layer between the surface and deeper layers. The seasonal pycnocline is typically marked by a sharp change in density over a small depth range on the order of meters. The sharp density change in the pycnocline acts as a barrier to energy exchange between the surface and deep layers. For a turbulent event to occur in the pycnocline, the inertial force driving the turbulence must overcome the strong restraining forces due to the sharp density change in the pycnocline. Activity in the seasonal pycnocline is generally controlled by interactions with mixing activity in the surface layer and the level of internal waves. Large-scale eddies and fronts can also trigger mixing activity in the seasonal pycnocline.

The main pycnocline is a broad, diffuse layer that separates the seasonal thermocline from the deep ocean. It is insulated from surface effects by the seasonal pycnocline and is marked by the ubiquitous presence of internal waves. In the open ocean, away from sources such as currents, seamounts, and islands, the major sources of activity in the main pycnocline are internal waves and near inertial frequency internal waves, large-scale horizontal eddies, and double-diffusive processes.

SOURCES OF MICROSTRUCTURE

Within the three general ocean depth regimes, different physical processes drive the occurrence of small-scale fluctuations in velocity, temperature, and salinity. The density stratification provides a restraining force that resists overturning. This restraining force is characterized by the Brunt–Väisälä frequency, defined by $N = (g/\rho)/(d\rho/dz)^{1/2}$ (where g is the gravitational constant and the z axis is positive down), which represents the frequency at which a water parcel would oscillate vertically about its equilibrium depth if the water parcel was adiabatically displaced. For a portion of the water column to overturn and produce turbulence and microstructure, the inertial forces of the physical process driving the overturn must exceed the resistant or buoyancy forces due to the stratification. Shear from internal waves and near inertial frequency internal waves, currents, fronts, and large-scale eddies can all generate small-scale activity through shear instabilities. Microstructure generated by shear instabilities is referred to as turbulence-induced microstructure. Double-diffusive convection depends on the local temperature and salinity contributions to the local density rather than the shear produced by larger-scale processes. Microstructure generated by double-diffusive convection is referred to as double-diffusive microstructure.

One particular type of shear instability is the Kelvin–Helmholtz shear instability or billows. Figure 2 shows a sequence of photographs of the time history of this type of instability as demonstrated[5] in a laboratory two-layer tank experiment. A density interface is subjected to a constant shear, producing billows that break down into turbulence and thicken the interface. The instability is characterized by the Richardson number, defined by $Ri = N^2/u_z^2$ (where u_z is the vertical shear of the horizontal velocity), which is the ratio of the buoyancy forces to the inertial forces. The theoretical threshold[6] for the inertial forces to overwhelm the restraining forces due to the density stratification is $Ri = 0.25$. Measurements of the Richardson number in the ocean show a cutoff at 0.25, indicating that Ri values less than 0.25 are not allowed to persist. Large shear values are observed in the regions above and below major current systems. In the open ocean away from sources such as seamounts and strong currents, the random supposition of shears due to internal waves and near inertial fequency internal waves intermittently generates shear values sufficient to induce turbulent mixing.[7]

Double-diffusive convection, a consequence of the large difference in the molecular diffusion rates of temperature (D_T) and salt (D_S), $D_T \approx 100 D_S$, has two distinct classes termed diffusive layering and salt fingering. Large regions of the ocean (e.g., the Central Waters of the Pacific and the Atlantic oceans, the Sargasso Sea, the Arctic Ocean, and the outfall of the Mediterranean Sea

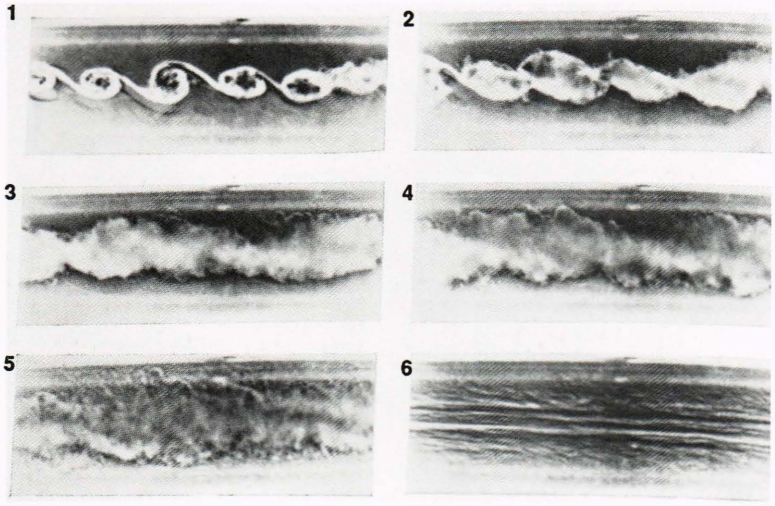

Figure 2. Time sequence of the formation and breakdown of a Kelvin–Helmholtz shear instability. The instability was generated by imposing a steady shear on a sharp density interface. The instability rolls up the interface into billows (1), which break down into a turbulent field (2–5) and thicken the interface (6). (Reprinted, with permission, from Ref. 5.)

in the Atlantic Ocean) have vertical gradients of temperature and salinity conducive to double-diffusive convection. Besides the sign of the vertical profiles of temperature and salinity, the relative contribution of temperature and salinity to the density plays a role in determining whether a double-diffusive instability can occur. The density ratio,[8] defined by $R_\rho = \alpha\Delta T/\beta\Delta S$, provides a measure of the potential for the occurrence of double-diffusive instabilities. The temperature and salinity difference is over a vertical interval. If temperature and salinity are both decreasing with depth and if $1 < R_\rho < 100$, then salt fingering may occur. If temperature and salinity are both increasing with depth and the density ratio is between $0 < R_\rho < 1$, then diffusive layering may occur. If $R_\rho \leq 0$, then the stratification is stable from a double-diffusive viewpoint. Turbulence is independent of the value of the density ratio. Temperature and salinity gradients in the upper Arctic Ocean increase with depth, favoring diffusive layering; temperature and salinity profiles often reveal a steplike structure called a thermohaline staircase, which is characteristic of diffusive layering. The general decrease with depth of the vertical gradients of temperature and salinity in the Sargasso Sea favors salt fingering. Since microstructure measurements discussed within this article have been derived from the Sargasso Sea, detailed discussion of double-diffusive processes will be limited to salt fingering.

A simple model of the salt fingering process starts with a stable stratification of warm, salty water overlaying cool, fresher water (temperature stable, salinity unstable, but density stable). The interface is given a sinusoidal perturbation, moving the cool, fresher water into the warm, salty layer, and the warm, salty water down into the cool, fresh layer. Heat diffuses from areas of high temperature to low temperature. Salt fingers grow in both directions since the upper layer warms the upward cool, fresher perturbations (become less dense), and the downward warm, salty perturbations cool (become more dense) as heat is lost from the perturbation to the colder, lower layer. Because of the slow diffusion rate of salt compared with temperature, salt fingers transport more salt than heat. Salt finger microstructure activity is patchy, limited in vertical extent, and in some ways appears similar to turbulence-generated microstructure. This intermittency or patchiness may be due to the random straining of the temperature and salinity profiles by internal waves. The random strain field of the internal waves can distort the temperature and salinity gradients such that the density ratio nears 1, enhancing the probability of double-diffusive convection. The observed intermittency of salt finger microstructure may also be due to the interleaving and incorporation of anomalous (in terms of the temperature–salinity relationship) small-scale water masses into the general water mass.[9]

Time series of salt fingering exhibit a narrowband, limited-amplitude appearance, whereas turbulence-generated microstructure exhibits a more wideband, variable-amplitude appearance. A shadowgraph[10] of a field of salt fingers generated in the double-diffusive tank in the APL Hydrodynamics Research Laboratory is shown in Figure 3. An internal wave propagates from left to right through the field of salt fingers, distorting the field of salt fingers from a vertical orientation toward a more horizontal orientation. The ubiquitous nature of internal waves in the ocean suggests that the same process occurs in the ocean. Note the regularity of the width of the "fingers" and the lack of variance at larger scales in the figure. If a temperature or conductivity sensor cut horizontally through the salt finger field, the time series would appear narrowband and limited in amplitude, even with the distortion of the salt finger field by the internal wave. The variance of the temperature and conductivity gradient spectra would be concentrated in a relatively narrow wavelength band about the 1-mm average horizontal wavelength of the salt fingers.

In stark contrast to the regular appearance of the salt finger field in Figure 3, Figure 4 demonstrates the irregular nature of turbulence and turbulence-induced microstructure. Fluorescein dye is injected through a grid in the Hydrodynamics Research Laboratory's recirculating flow channel, and a laser sheet is used to induce the dye to fluoresce over the 88 cm × 56 cm cross section of the channel. A wide range of dye scales is visible. The velocity field created by the grid stirs and strains the dye

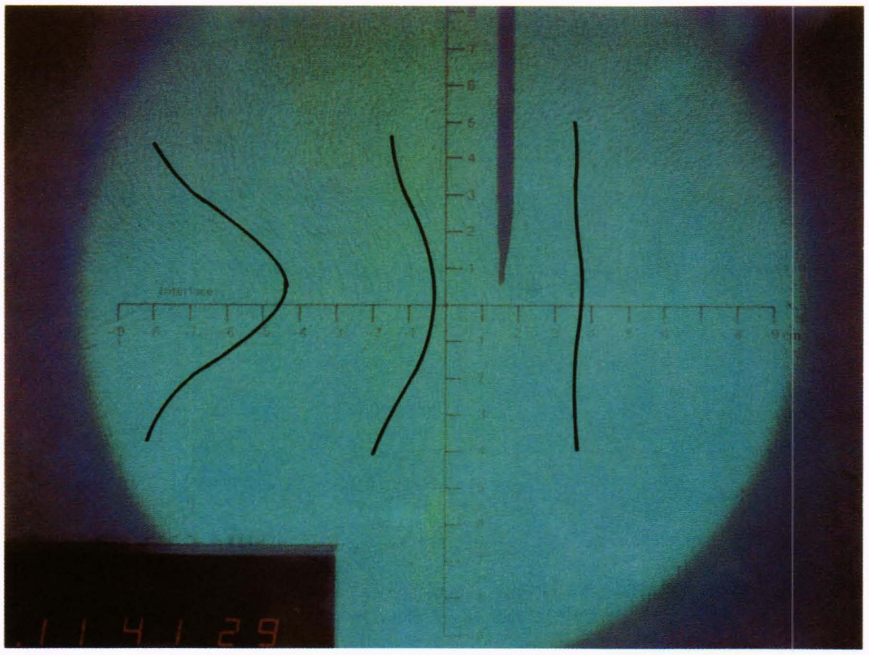

Figure 3. Salt finger field created in the double-diffusive tank in the APL Hydrodynamics Research Laboratory[10] to study the interaction of internal waves with salt fingers. An internal wave propagates from left to right, straining and distorting the salt finger field. The horizontal scale of the vertically oriented salt fingers is about 1 mm. (For reference, a scale in centimeters is shown.)

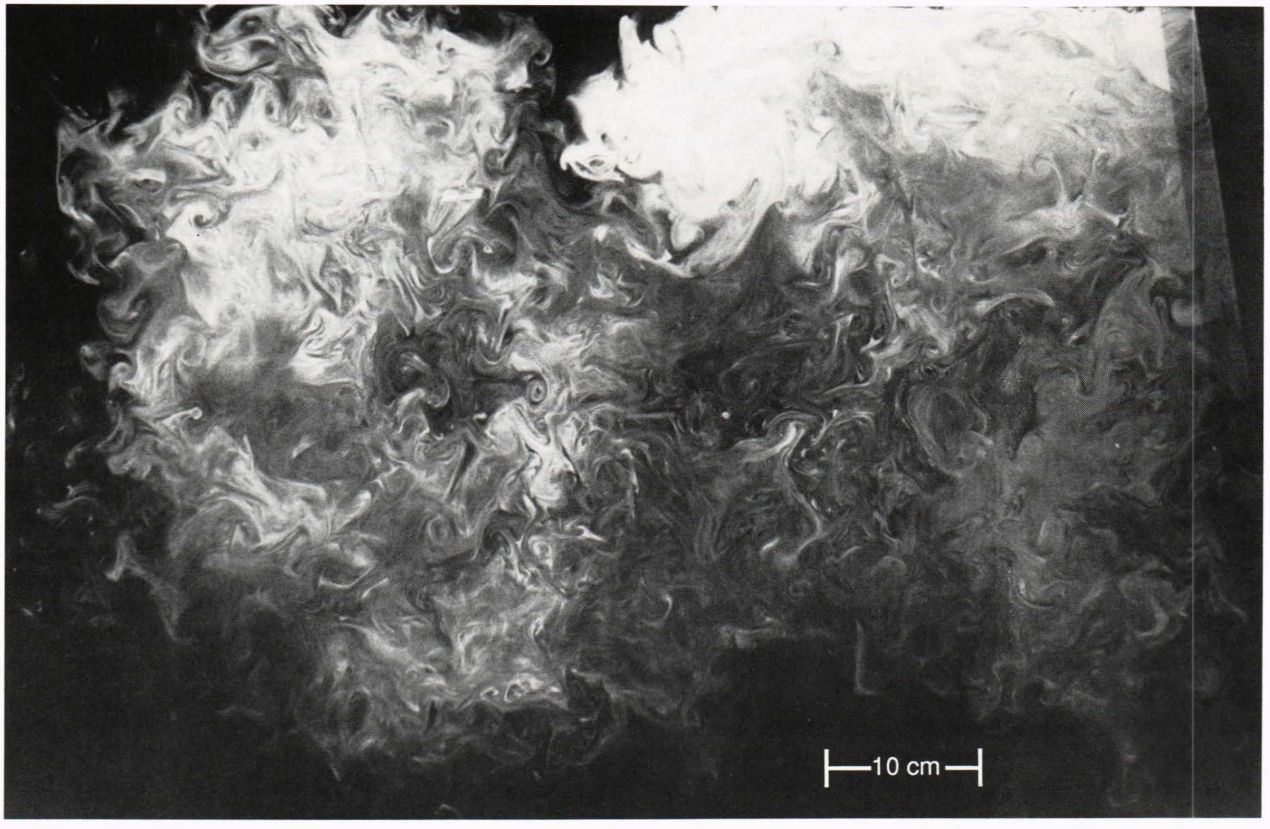

Figure 4. Turbulence-induced microstructure produced in the Hydrodynamics Research Laboratory's recirculating flow channel. Fluorescein dye injected from a grid upstream and illuminated by a laser sheet across the 88 cm × 56 cm cross section of the channel visually demonstrates the wide range of scales present in turbulence-induced microstructure.

field. Dye scales much smaller than any turbulent velocity scale are created by the straining action of the small-scale eddies. The largest isotropic eddy generated by the grid is about 10 cm (grid rod spacing is 10 cm). Based on the turbulence levels of the velocity field measured by a hot-film anemometer, the smallest turbulent scale is about 1 cm, and the smallest dye wavelength would be about 0.03 cm, which implies that more than two decades

of dye scales are present. Since fluorescein dye is salt-based, the contrast and small-scale detail apparent in Figure 4 are representative of a patch of salinity microstructure. A patch of temperature microstructure, on the other hand, would have less contrast because of the smoothing effect of the higher molecular diffusion rate of temperature compared with salt. The measured turbulence levels are comparable to active turbulent patches in the ocean.

The kinetic energy of the turbulence is finally dissipated (converted into heat) at the smallest scales of the turbulence, where the inertial forces become equal to viscous forces. Much as the stratification provides a force resistant to the vertical rotation of larger scales of the turbulence, the viscosity of the water provides a force that impedes the rotation in any direction of smaller scales and limits the transfer of energy to smaller scales. Turbulence in the ocean is characterized by the kinetic energy dissipation rate, ϵ, which is a measure of the intensity of the turbulence and is proportional to the variance of the small-scale velocity gradient field. Typical turbulent velocity scales for ocean turbulence patches are on the order of a few meters to about a centimeter. Turbulence stirs and strains the temperature (or salinity and conductivity) field to small scales. Molecular diffusion of temperature acts to reduce and limit the high-gradient regions produced by the straining action of the turbulence on the temperature field. Microstructure activity in the ocean induced by turbulence is characterized by the dissipation rate of temperature variance, χ_T, which is the counterpart of the kinetic energy dissipation rate for the temperature field and is proportional to the variance of the small-scale temperature gradient field. Typical scales for temperature microstructure are on the order of a meter to millimeters.

Oceanic measurements of ϵ are usually obtained using vertical profilers equipped with airfoil probes that sense the velocity components orthogonal to the vertical profile. The airfoil probes are piezoelectric beams, similar to a phonograph needle. The transverse deflections of the piezoelectric beam produce a voltage proportional to velocity. The voltages are usually analog-differentiated, thus generating a signal proportional to the velocity gradient. Thermistors and conductivity sensors are used to measure χ_T. Without large corrections for sensor response, thermistors and conductivity sensors often cannot resolve the millimeter scales of the temperature gradient field required to accurately estimate χ_T. Estimates of the bandpassed temperature gradient variance are often used to characterize microstructure activity.

An example of the intermittent distribution of microstructure activity in the ocean is shown in Figure 5. The two-dimensional slice (15 m $\times$ 2.2 km) of microstructure activity was derived[11] from towed conductivity chain measurements in the Sargasso Sea obtained during an APL field test in November 1984. The time series for each sensor represents pre-emphasized conductivity (conductivity plus the derivative of conductivity) and is plotted in a min/max format. The vertical motion of the towed chain is indicated by the bottom trace. The time series are marked by the intermittent occurrence of microstructure activity. Large portions of the segment have no discernible microstructure activity. Five patch groups are highlighted in Figure 5. (A patch group is defined as a spatially contiguous set of patches.) Patch groups 1 and 2 have the narrowband, limited-amplitude characteristics of salt fingering. Patch groups 3 and 4 have the wideband, highly variable amplitudes characteristic of turbulence-induced microstructure. It is unclear from a visual inspection whether patch group 5 is due to salt fingering or turbulence. Blowups of single-sensor cuts through patch groups 1 (salt fingering) and 3 (microstructure created by turbulence) in Figure 6 show the differences in the appearance of the time series of the two processes. Statistical discrimination techniques using these differences to determine whether a patch of microstructure is due to salt fingering or turbulence will be discussed in detail later in this article.

TURBULENCE AND MICROSTRUCTURE STATISTICS: IMPLICATIONS OF LOGNORMALITY AND INTERMITTENCY

Some important issues in oceanography concern the average turbulence and microstructure levels for a given ocean volume (area and layer) and the large-scale processes forcing the small-scale activity. These average levels affect the vertical diffusion rates of passive scalars such as temperature, oxygen, and nutrients, which are important for microorganisms. In addition, turbulent dissipation of kinetic energy is an important factor in modeling large-scale currents such as the equatorial undercurrent. To form a meaningful estimate of the mean levels and calculate the associated uncertainty, the underlying distribution of the turbulence and microstructure must be considered. The probability distribution of the magnitude of turbulence and microstructure statistics determines which sampling strategies are appropriate and which estimators should be used to calculate parameters such as the mean value. Variability of the statistics of turbulence and microstructure in space and time is inherent since the underlying process driving the small-scale activity generally varies slowly in space and time. Because of the typical 100 to 1 aspect ratio of vertical to horizontal density gradients (with the exception of fronts) and the physics of the large-scale sources, the sources and the available energy for small-scale mixing change with depth much more than with horizontal distance. Even in a given layer, variability of the source with time should be considered.

Statistics of Microstructure Parameters

Probability distributions that are approximately lognormal are typically observed[12] for ϵ, χ_T, and bandpassed temperature gradient variance (see the boxed insert for a review of the lognormal distribution). If a random variable x such as ϵ, χ_T, or bandpassed temperature gradient variance is lognormally distributed, then $\ln(x)$ is Gaussian-distributed with expected value μ and variance σ^2. Several factors must be considered before testing a sample set for lognormality (or any distribution). Is the sample set composed of independent, identically distributed (from the same parent population) random variables?

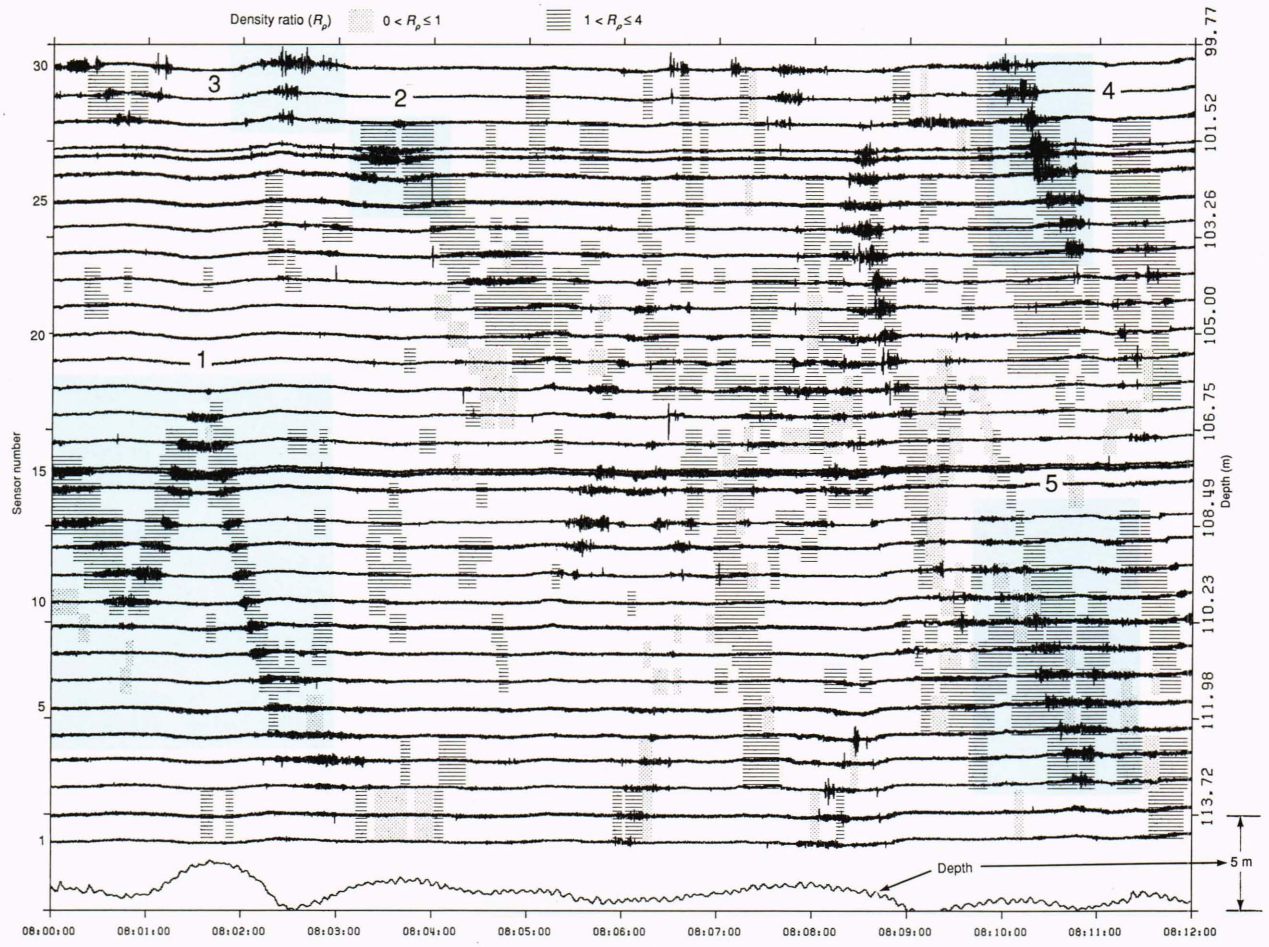

Figure 5. A 15 m × 2.2 km segment of pre-emphasized min/max conductivity from the towed chain data taken from below the seasonal thermocline in the Sargasso Sea. The depth variation of the towed chain is shown by the bottom trace. The microstructure is distributed intermittently throughout the segment (computer-generated material, Ref. 11). Five patch groups are highlighted. The appearance of patch groups 1 and 2 is consistent with salt fingering as the source. Patch groups 3 and 4 appeared to be microstructure generated by turbulence. The source of patch group 5 is not clear visually. It could be salt fingering, turbulence, or a mixture of both. The density ratio is gray-scaled for the microstructure patches.

Comparisons to the lognormal distribution should be restricted to layers and volumes where the underlying physical process driving the mixing activity is stationary over the sample period. If the sample set passes statistical tests for these criteria, and if no noise contamination of the data is present, then and only then is it fair to test the data against the lognormal distribution and conclude that failure to agree with lognormal is significant. If system noise contamination exists, then the sample set has to be tested against a distribution based on the combined lognormal and noise distributions rather than just the lognormal distribution.

The high-frequency or wave-number measurement requirements for turbulence and microstructure observations typically lead to contamination by instrument noise. Monte Carlo simulations[12] indicate the departures from lognormality at small values frequently observed in evaluations of ocean turbulence, and microstructure measurements are consistent with instrument noise. The measured data are assumed to be represented by the sum of a lognormal random variable and a chi-squared noise random variable.[12] The ensuing cumulative distribution function (CDF) results from the convolution of the lognormal and noise probability density functions (PDF's), implying that the noise contamination will occur over a range of values and not just at a sharp cutoff point. The underlying ocean is assumed to be represented by the linear portion of the CDF (Gaussian CDF plots as a straight line on Gaussian probability paper) uncontaminated by instrument noise. If significant instrument noise contamination is present, then the arithmetic mean and standard deviation, m and s, yield poor estimates of the underlying μ and σ. By using the linear region to estimate μ and σ, the effects of instrument noise on the statistics are reduced.

The histogram and CDF from towed chain data taken in the seasonal thermocline of the Sargasso Sea are shown in Figure 7. The CDF is based on 3-m samples of the logarithm of bandpassed (3- to 0.05-m) conductivity gradient variance. The CDF is plotted against a $\log_{10}$ and natural log axis on Gaussian probability paper. The histogram is shown in the upper portion of the figure. The

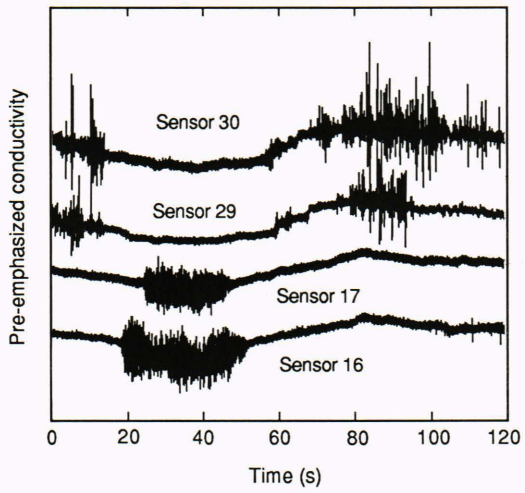

Figure 6. Blowup of single-sensor time series from patch groups 1 (salt fingering, sensors 16 and 17) and 3 (turbulence-induced microstructure, sensors 29 and 30). The salt finger time series is limited in amplitude. The turbulence-induced time series displays highly variable amplitudes.

corresponding CDF is shown by the black curve in the lower portion of the figure. The lognormal CDF and PDF predicted by the standard arithmetic estimators m and s are shown by the green curves and show poor agreement with the measured CDF and histogram. The blue curve on the CDF plot indicates the underlying lognormal distribution according to the lognormal plus noise model. The PDF (blue curve) predicted by the linear region displays excellent agreement with the histogram over the range where the data are not noise-contaminated. A Monte Carlo simulation based on the lognormal plus noise model is shown by the red curve on the CDF plot. The Monte Carlo simulation is based on the lognormal distribution estimated from the linear region and instrument noise contamination derived from noise spectra. The agreement between the measured and simulated CDF's is excellent and indicates that the departure at the low-magnitude end is consistent with system noise. The maximum likelihood estimate of the expected value (see the boxed insert) of the conductivity gradient variance is 1.6×10^{-4} (mmho/cm/m)^2. The mean-to-median ratio is about 12, and the mean-to-mode ratio is 1856.

Intermittency of Microstructure

Describing their definition of "intermittent," Monin and Yaglom[13] note "This word is meant to denote the tendency of small-scale turbulence to concentrate into individual 'bunches' surrounded by extensive flow regions in which there are only much smoother large-scale disturbances (or perhaps no disturbances at all)." Their statement accurately describes the temporally and spatially intermittent occurrence of patches of small-scale turbulence and microstructure in the ocean such as those observed for the towed chain segment seen in Figure 5. Kolmogorov addressed the issue of the intermittency of ϵ in turbulence measurements with his third hypothesis.[14] According to Kolmogorov, the intermittency factor, $\sigma^2_{\ln \epsilon_r}$, is related to the external turbulent length scale L by

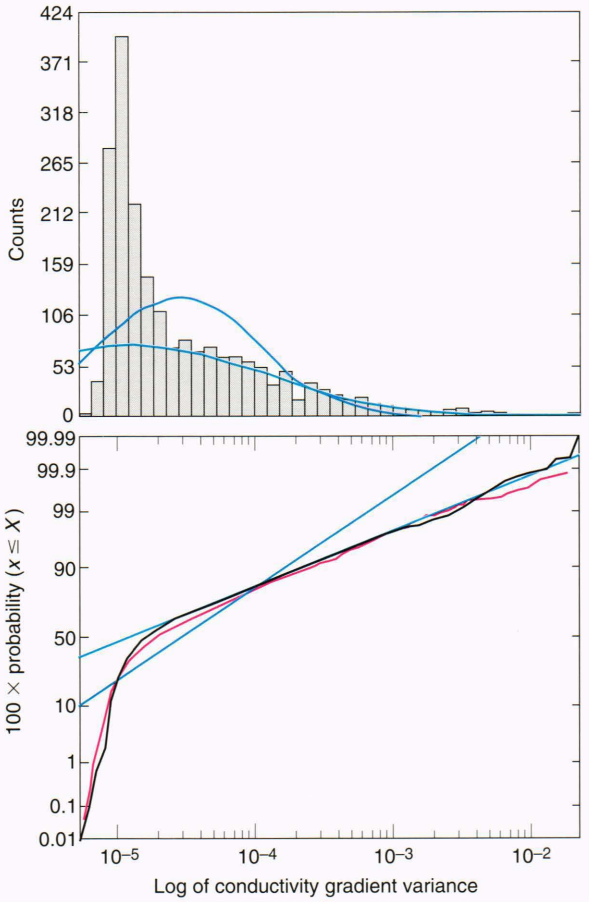

Figure 7. Lognormal evaluation of the logarithm of conductivity gradient variance computed from the 3- to 0.05-m wavelength band. The black curve in the lower portion corresponds to the measured cumulative distribution function (CDF), and the histogram is shown in the upper figure. The green curves correspond to the lognormal distribution estimated by the standard arithmetic mean and standard deviation. Poor agreement with the measured functions is observed. The blue curves in the upper and lower portions correspond to the lognormal distribution estimated from the linear region of the CDF. The agreement of the estimated lognormal distribution with the measured histogram is excellent over the region not contaminated by system noise. The Monte Carlo simulation (red curve), assuming a lognormal plus noise random variable, displays excellent agreement with the measured CDF.

$$\sigma^2_{\ln \epsilon_r} = A(\mathbf{x}, t) + \mu_\epsilon \ln(L/r) , \qquad (1)$$

where $A(\mathbf{x}, t)$ represents a function that depends on the characteristics of the large-scale motions, μ_ϵ is the universal Kolmogorov constant (measurements range from 0.3 to 0.5), and r represents the scale over which ϵ is averaged. The magnitude of the external length L is related to the scale of the forcing function represented by $A(\mathbf{x}, t)$. From Equation 1, the larger the external length scale of the turbulence, the larger the intermittency. Kolmogorov's hypothesis for the intermittency of the kinetic energy dissipation rate has been extended to the intermittency of the dissipation rate of temperature variance.[13,15]

The factor $\sigma^2_{\ln}$ has been labeled the intermittency factor[12] since the larger the underlying value of $\sigma^2_{\ln}$, the larger the intermittency of the intensity of turbulence and

THE LOGNORMAL DISTRIBUTION

If a random variable x is lognormally distributed, then $\ln(x)$ is Gaussian-distributed with expected value μ and variance σ^2. The probability density function (PDF) for x is given by

$$\mathrm{PDF}(x) = \frac{1}{x\sigma\sqrt{2\pi}} \exp\left\{\frac{-[\ln(x) - \mu]^2}{2\sigma^2}\right\}, \quad (1)$$

where μ and σ^2 are the expected value and variance, respectively, of $\ln(x)$. The expected value of x is given by $\exp(\mu + \sigma^2/2)$. The median and the mode of x are given by $\exp(\mu)$ and $\exp(\mu - \sigma^2)$, respectively. The mean-to-mode value for lognormal distributions is given by $\exp(3\sigma^2/2)$. The mean > median > mode, unlike Gaussian random variables, wherein the mean = median = mode.

An example of a lognormal PDF(x) is shown in the figure (top) along with the corresponding $\ln(x)$ Gaussian PDF. The PDF for this example is based on the μ (1.73) and σ (0.37) estimated from the variable ln(kurtosis) for the turbulence control patches discussed in the text (Table 1). The mean, median, mode, and mean-to-mode ratios (assuming lognormality) are given by 6.0, 5.6, 4.9, and 1.22, respectively. The lognormal PDF is positively skewed with a relatively short upper-magnitude tail. The left and right ordinate axes correspond to the magnitude of the lognormal and Gaussian PDF's, respectively. The upper and lower abscissas correspond to the x values (for the lognormal PDF) and the $\ln(x)$ values (Gaussian PDF), respectively. A second example of a lognormal PDF and the corresponding Gaussian PDF is also displayed (bottom) for the same μ, but with a σ value of 2.24 that is representative of the values of σ observed for ϵ, χ_T, and bandpassed temperature variance (text, Fig. 6) in the seasonal thermocline. Now the mean, median, mode, and mean-to-mode ratios are given by 69, 5.6, 0.04, and 1856, respectively. The lognormal PDF is strongly positively skewed with a long upper-magnitude tail.

Another difference between lognormal and Gaussian-distributed random variables is how to best estimate such parameters as the expected value. Unlike the Gaussian distribution where the arithmetic mean is the maximum likelihood estimator of the expected value, the maximum likelihood estimator[29] of the expected value for a lognormal random variable, X_{mle}, is given by $\exp(m + s^2/2)$, where m and s are defined by

$$m = \frac{1}{M}\sum_{i=1}^{M} \ln(x_i) \quad (2)$$

and

$$s^2 = \frac{1}{M}\sum_{i=1}^{M} [\ln(x_i) - m]^2 \quad (3)$$

and are the standard arithmetic estimates of μ and σ^2. Typically, M (number of samples) is replaced by $M - 1$ in Equation 3 to yield an unbiased estimate of σ^2. Although the arithmetic mean of x has theoretical confidence limits only for the asymptotic case of a large number of samples, theoretical confidence intervals are available[12] for the maximum likelihood estimator.

The estimated expected values from small data sets with large σ^2 factors are likely to reflect estimates of the mode (most probable value) rather than the mean. One consequence of a lognormal-distributed random variable with a large variance is that a large number of samples are required for the arithmetic mean to converge to the expected value compared with the number of samples required for a Gaussian-distributed random variable. If the distribution is lognormal, but the data have only a small variance, the expected value can be accurately estimated by the arithmetic mean from a small number of samples.

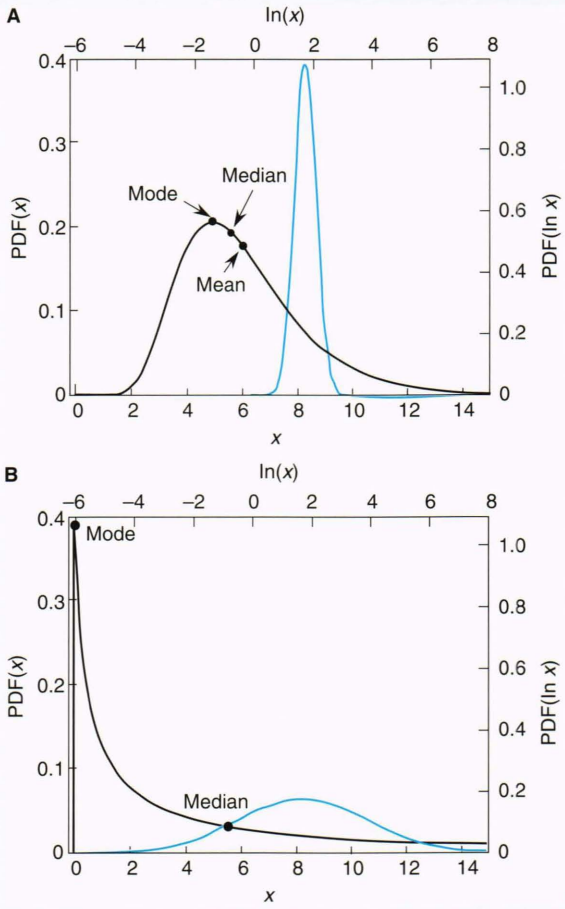

Two examples of lognormal PDF's (x) (black curves) and their corresponding Gaussian PDF's (ln x) (blue curves). **A.** $\mu = 1.73$; $\sigma = 0.37$. **B.** $\mu = 1.73$; $\sigma = 2.24$. The mean value of 69 would be well off to the right for B. The strong dependence of the lognormal distribution function on σ can be seen by the lengthy upper-magnitude tail (large positive skewness) exhibited in B compared with A.

microstructure in both space and time. Measurements of ϵ in surface mixing layers tend to have small intermittency factors (1 to 2) relative to measurements in the seasonal pycnocline. Since the vertical temperature gradient is usually small in the surface layer, making measurements of χ_T difficult, χ_T values are usually reported from depths below the surface layer. Measurements of both ϵ and χ_T in the seasonal pycnocline typically display large intermittency factors (3 to 7).[12] This variation of $\sigma^2_{\ln}$ with depth implies that fewer samples are required in the surface layer compared with the seasonal or main pycnocline in order to accurately estimate the expected value.

The intermittency of microstructure can also be examined from the spatial distribution of microstructure activity. The statistics of the horizontal and vertical extent of microstructure patch groups were examined[16] using 200 km of towed thermistor data taken in the seasonal pycnocline of the Sargasso Sea in November 1982. The 200 thermistors on the towed chain were spaced at 5-cm intervals and covered an aperture of 10 m. Patches observed on adjacent sensors are placed in the same patch group if the patches overlap horizontally. The average aspect ratio (width to height) of a microstructure patch group was about 200; widths and heights ranged from 20 m to 1 km and 5 cm to 5 m, respectively. The average width and height of the microstructure patch groups were 120 m and 55 cm, respectively. The spatial intermittency of the microstructure is highlighted by the observation that microstructure patches constituted only 6.9% of the data, and over 95% of the patches were less than 2 m tall.

The spatial characteristics of microstructure patches should be considered in sampling strategies. Investigators must recognize that large data sets are usually required for intermittent variables such as turbulence and microstructure statistics. Assumption of lognormality and the intermittency factor σ^2 provide a framework for estimating how many independent samples are required to resolve the distribution. Separation of the microstructure into two classes, turbulence-induced microstructure and salt fingering, is addressed in the next section.

DISCRIMINATION BETWEEN TURBULENCE-INDUCED MICROSTRUCTURE AND SALT FINGERING

Investigators are trying to tie small-scale activity to large-scale processes to ascertain the importance of a given large-scale process for a given ocean volume and for the overall oceanic system. Unconditional distribution functions for microstructure parameters do not provide information that allows discrimination between microstructure due to salt fingering and that due to turbulence. The Laboratory is investigating discrimination techniques based on the temperature and salinity fields and the internal statistical and spectral characteristics of the microstructure. The density ratio, based on the local temperature and salinity gradients, helps to identify where salt fingering microstructure would be likely, but does not provide a clear distinction between double-diffusive and turbulence-induced microstructure when $R_\rho > 0$. The wideband and highly variable amplitudes that are characteristic of turbulence-induced microstructure versus the narrowband, limited-amplitude appearance of salt finger microstructure imply that the kurtosis[17] and the spectral slope of the temperature or conductivity gradient spectrum may help to distinguish between turbulence-induced microstructure and salt fingering. (Kurtosis is discussed in detail later in this article.) The towed segment presented in Figure 5 is used in this section to evaluate each of these statistics as discriminants.

Density Ratio as a Discriminant

Theoretical predictions[18,19] indicate an enhanced growth rate of salt fingers as R_ρ approaches 1. Microstructure measurements[11,20,21] from vertical profiles and towed chain measurements obtained during several APL field tests in a variety of areas (Sargasso Sea, off San Diego near San Clemente Island, and the Tongue of the Ocean) that were conditionally sampled on R_ρ showed a significant increase in microstructure activity when R_ρ approached 1. The unconditional and conditional histograms[21] derived from 260 km of towed temperature and conductivity chain measurements are displayed in the upper plot of Figure 8. A cell of the unconditional histogram represents all the 1-s (≈3-m) samples that fell within the given density ratio bin. The conditional histogram is conditioned on the presence of microstructure activity. The probability of microstructure activity, generated by dividing the conditional histogram by the un-

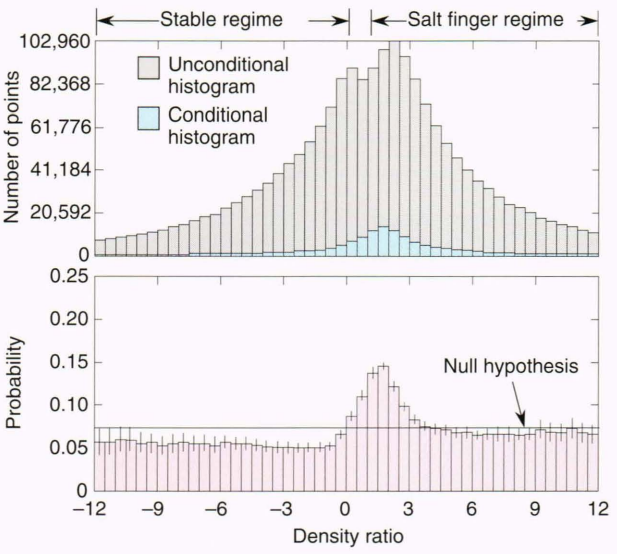

Figure 8. The ratio of the unconditional histogram (all samples) divided by the histogram conditioned on zero crossings ≥ 2 (microstructure) plotted as a function of density ratio.[21] An increased probability of microstructure is observed for $0 < R_\rho < 4$. Double-diffusive convection requires density ratios between 0 and 100. Since turbulence-induced microstructure should be independent of the density ratio, the flat level observed for $R_\rho < 0$ should extend to $R_\rho > 0$, indicating the relative proportion of microstructure due to turbulence (73%) and double-diffusive convection (27%). (Cell width = 0.50; 90% confidence [N/12]; number of points = 2,436,100; number of conditional points = 180,433; total probability = 0.074.)

conditional histogram, is enhanced for R_ρ near 1. The relatively uniform probability of microstructure activity for R_ρ less than zero (non–double-diffusive regime) should extend over the positive R_ρ values (double-diffusive regime), since turbulence caused by shear instabilities should be independent of R_ρ. Assuming this is true, Figure 8 suggests that 27% of the microstructure activity was due to double diffusion.

To illustrate the use as well as the limitations of using density ratio to determine whether salt fingering or turbulence is the source for individual patches of microstructure, we return to Figure 5. Gray scales corresponding to limited ranges of R_ρ—$0 < R_\rho \leq 1$ (diffusive) and $1 < R_\rho \leq 4$ (salt finger)—are displayed in conjunction with the microstructure activity. Patch groups 1 and 2 generally have density ratios between 1 and 4 and display the narrowband, limited-amplitude appearance of salt fingering. Hence, a good correlation between salt fingering and R_ρ values in the salt finger regime occurs. Patch group 3 has the variable amplitude consistent with turbulence-induced microstructure and R_ρ values outside the double-diffusive convection regime. Patch group 4 has R_ρ values between 1 and 4, but shows the wideband and highly variable amplitude typical of turbulence-induced microstructure. Patch group 5 has the right density ratio for salt fingering, but it is unclear visually whether the source is salt fingering or turbulence. More robust statistical approaches to discriminating between salt fingering and turbulence sources of microstructure are required and are the subject of the following discussion.

Kurtosis as a Discriminant

Kurtosis, K, is a measure of the weight of the tails of the probability distribution and is defined for small-scale conductivity gradient data (demeaned) by

$$K = \frac{\langle (C_x)^4 \rangle}{\langle (C_x)^2 \rangle^2} , \qquad (2)$$

where C_x is the small-scale conductivity gradient. The narrowband nature of salt fingering leads to a small kurtosis on the order of 3 (Gaussian random variables have a kurtosis of 3), whereas the highly variable amplitudes characteristic of microstructure due to turbulence typically produce kurtosis values on the order of 6.

To statistically discriminate between salt fingering and turbulence as the source of the microstructure, the probability density function (PDF) of kurtosis is required for each process. Investigators at APL have generated PDF's of kurtosis from localized regions (control patches) identified as turbulence-induced microstructure or salt fingering from towed chain segments obtained during a November 1984 field test in the Sargasso Sea. The selection of the control patches was based in part on R_ρ and the visual characteristics of the time series. The mean kurtosis estimates of 6 and 3 for the turbulence-induced microstructure and salt finger control patches, respectively, are consistent with measurements by other investigators.[22,23] The means and standard deviations of the kurtosis estimates for the control patches are summarized in Table 1. The minimum overlap between the salt finger and turbulence PDF's occurred at a kurtosis value of 4, which is used as the gray scale threshold in Figure 9 to separate the two processes. The microstructure activity is identified as salt fingering for kurtosis values ≤4 and is attributed to turbulence for kurtosis values >4. Patch group 1 was used as the control region to estimate the PDF of kurtosis for salt fingering. The kurtosis values of patch group 2 are completely consistent with salt fingering, and the kurtosis values of patch group 3 are consistent with turbulence-induced microstructure. Patch groups 4 and 5 are dominated by kurtosis values greater than 4, consistent with turbulence-induced microstructure, even though the density ratio values are between 1 and 4, which would suggest salt fingering as the source of the activity. Hence, kurtosis can be used to discriminate between turbulence-induced microstructure and salt fingering, and it improves upon the use of density ratio, particularly where R_ρ values could support either turbulence or salt fingering.

Spectral Slope as a Discriminant

Theoretical modeling[24] of the turbulence-induced temperature gradient spectrum predicts a temperature gradient spectral wave-number dependence of k^1 (slope of 1 on a log–log plot) over the range of scales before molecular diffusion of temperature induces a roll-off in the spectrum. Measurements, both in the ocean and laboratory experiments, confirm the existence of the Batchelor spectrum.[25–27] In contrast to the wideband nature of microstructure created by turbulence, salt fingering has preferred scales on the order of a few centimeters. Lack of variance at large scales leads to a steep temperature or conductivity gradient spectrum with a spectral slope that significantly exceeds 1. Spectra generated from a salt finger spectral model[9] and microstructure observations[9,21–23] yield spectral slopes of about 2 for salt fingering patches.

The same control patches used to estimate the PDF's of kurtosis for turbulence-induced microstructure and salt fingering were used to estimate the PDF's of spectral slope for each source.[11] The means and standard deviations of the spectral slopes for the control patches are summarized in Table 1. Figure 10 displays gray scales of spectral slope in conjunction with the microstructure activity for the same segment of data shown in Figure 5. The microstructure activity is identified as due to turbulence for spectral slopes ≤1.2 and as salt fingering for spectral slopes >1.2. The minimum overlap between the salt finger and turbulence PDF's occurred at a spectral slope value of 1.2. Spectral slopes for patch group 2 are consistent with salt

Table 1. Summary of the means (μ) and standard deviations (σ) of spectral slope, ln(kurtosis), and kurtosis for turbulence-induced microstructure and salt finger control patches.[11]

	Spectral slope		ln(kurtosis)		Kurtosis	
Control patches	μ	σ	μ	σ	μ	σ
Salt finger	1.50	0.26	1.15	0.15	3.18	0.56
Turbulence	0.72	0.34	1.73	0.37	6.11	3.4

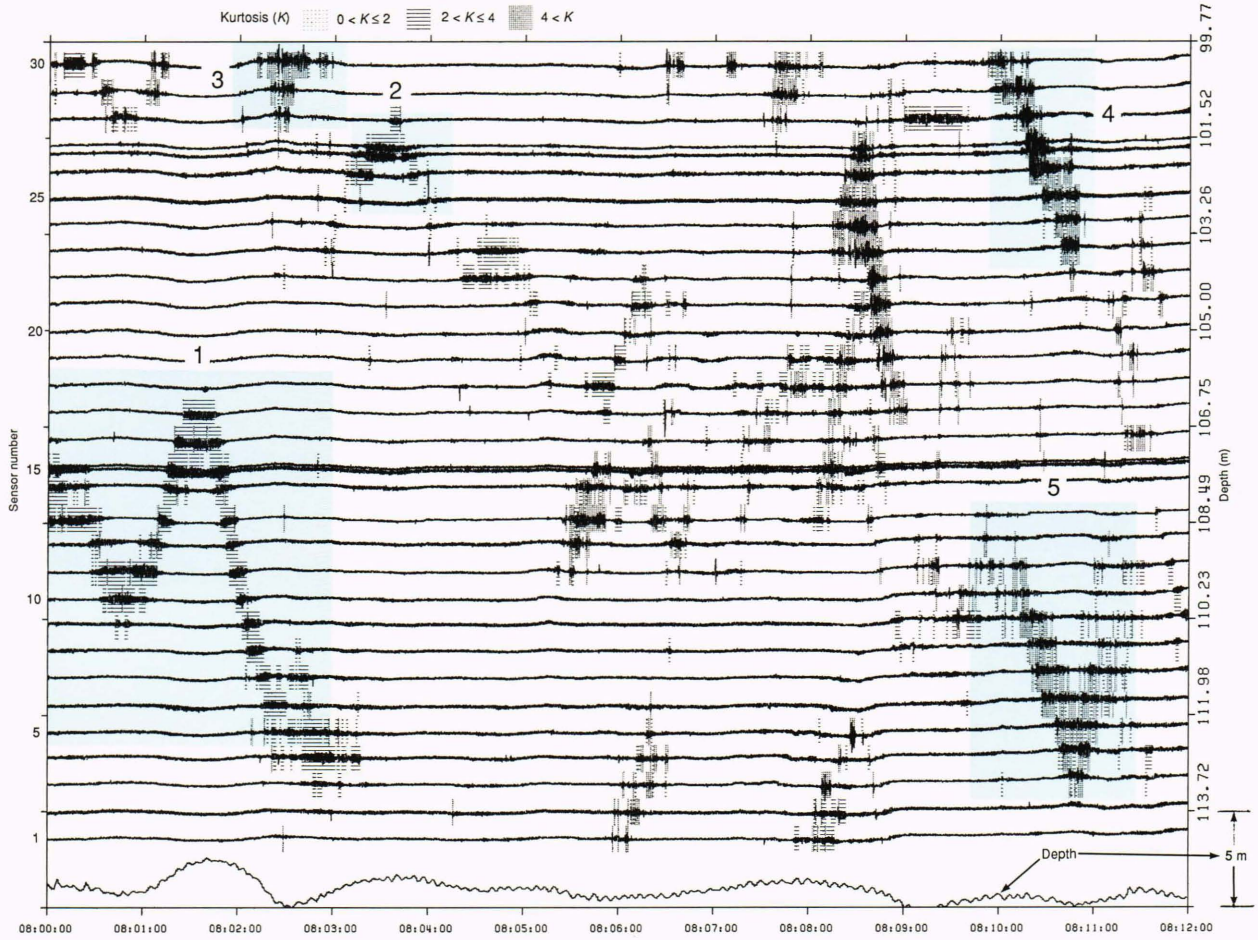

Figure 9. Kurtosis is gray-scaled for the same data segment shown in Figure 5 (computer-generated material, Ref 11). Patch group 2 has kurtosis values consistent with salt fingering. Kurtosis in patch groups 3 and 4 is dominated by values consistent with turbulence-induced microstructure. Kurtosis values for most of the microstructure in patch group 5 are consistent with turbulence-induced microstructure, but a small intermittent fraction appears to be in the range expected for salt fingering. Spatial mixtures are quite possible.

fingering; those for patch groups 3, 4, and 5 are consistent with turbulence-induced microstructure. Spectral slope also improves upon the use of density ratio as a discriminant.

The Log-Likelihood Approach to Discrimination

Under current investigation[11] at APL is an optimal discrimination approach based on a statistic called the log-likelihood ratio[28] λ, defined for a simple random variable x as

$$\lambda = \ln\left[\frac{P(x|SF)}{P(x|Turb)}\right], \qquad (3)$$

where P(x|SF) and P(x|Turb) are the PDF's of x given salt fingering and turbulence, respectively. The likelihood ratio technique is a formalism for minimizing the errors in decision making by using the ratio of the PDF's for the observables that have different distributions in salt fingering and turbulence. It is commonly used in hypothesis testing and provides a quantitative measure of decision making as well as estimates of the error in the decision (e.g., probability of incorrectly identifying a sample as coming from the salt finger distribution when it really comes from the turbulence distribution).

For $\lambda > 0$, the log-likelihood ratio would identify a patch as due to salt fingering; for $\lambda < 0$, the patch would be identified as due to turbulence; and for $\lambda = 0$, salt fingering or turbulence would be equally probable. This optimal discrimination approach can be extended to multiple variables (e.g., slope and kurtosis). For ease of implementation, a Gaussian model is commonly used for the parameters when warranted. In such cases the bivariate distributions are uniquely determined by the means, standard deviations, and correlation coefficients. Although the spectral slope PDF's for either salt fingering or turbulence are nearly Gaussian, the kurtosis PDF's for turbulence have many larger values, causing the distribution to be non-Gaussian. The distribution can be made more nearly Gaussian by taking the natural logarithm of the kurtosis.[11,27] Hence, the log-likelihood ratio for a two-parameter—slope, ln(kurtosis)—system can be written as

$$\lambda = \ln\left\{\frac{P[S, \ln(K)|SF]}{P[S, \ln(K)|Turb]}\right\}, \qquad (4)$$

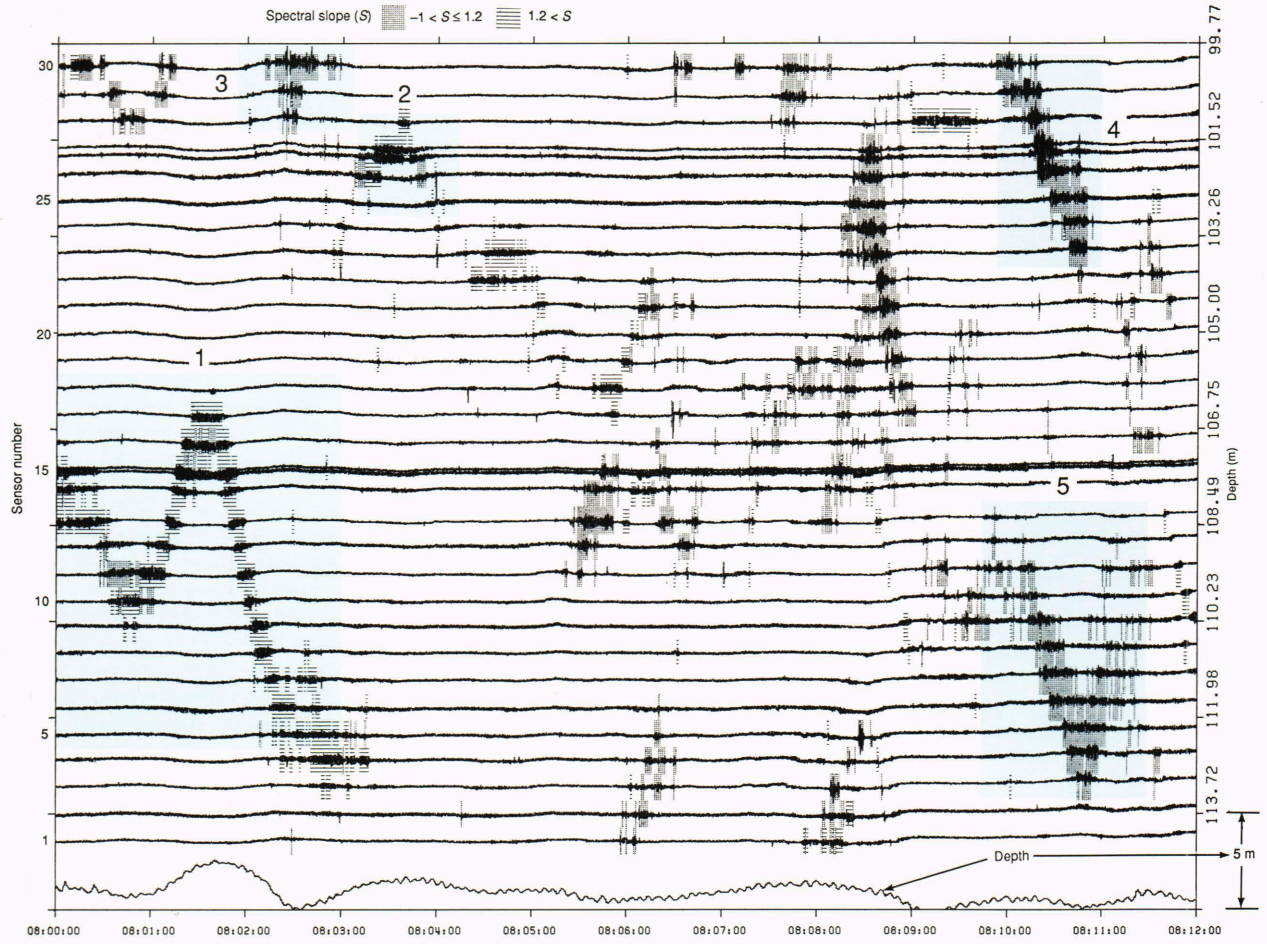

Figure 10. Spectral slope is gray-scaled for the microstructure patches for the same data segment shown in Figure 5 (computer-generated material, Ref. 11). Patch group 2 has spectral slopes consistent with salt fingering. Patch groups 3, 4, and 5 have spectral slopes consistent with turbulence-induced microstructure.

where P[S, ln(K)|SF] and P[S, ln(K)|Turb] are the joint Gaussian PDF's of spectral slope and ln(kurtosis) for salt fingering and turbulence, respectively.

To characterize the joint PDF's presented in Equation 4, the PDF's of ln(kurtosis) were generated for each source from the same control patches used previously to estimate the PDF's of kurtosis and spectral slope. The PDF's of ln(kurtosis) appeared more Gaussian for each source than the PDF's of kurtosis. The means and standard deviations of spectral slope, ln(kurtosis), and kurtosis for each test segment are summarized in Table 1.

The log-likelihood approach of combining spectral slope and ln(kurtosis) offers the possibility of improving discrimination between turbulence-induced microstructure and salt fingering for patches such as those in patch group 5. Just as the success of the univariate discriminants kurtosis and spectral slope depended on the degree of overlap between the PDF's for each source, the success of the log-likelihood approach also depends on the degree of overlap between the joint PDF's based on spectral slope and ln(kurtosis) for turbulence-induced microstructure and salt fingering. The log-likelihood ratio technique, however, should minimize errors in discrimination and present an excellent opportunity for properly characterizing large regions of ocean.

CONCLUSIONS

The Johns Hopkins University Applied Physics Laboratory has been involved in studies of small-scale mixing activity in the ocean for over a decade. Microstructure activity is distributed intermittently throughout the ocean. The data sets gathered during APL field tests in the Sargasso Sea provide the large sample base required to test hypotheses concerning the distribution functions of microstructure and the relative contributions of turbulence-induced microstructure and salt fingers to the overall microstructure. Monte Carlo simulations indicate that the probability density functions of bandpassed temperature gradient variance are consistent with lognormal distribution functions. Heights of microstructure patches are typically on the order of a meter with aspect ratios (width to height) on the order of 200. Significant advances have been made in developing statistical techniques to discriminate between salt fingering and microstructure created by turbulence. Discrimination results based on the

univariate statistics of density ratio, spectral slope, and kurtosis indicate that spectral slope and kurtosis improve upon the use of the density ratio as a discriminant. An optimal bivariate method of discrimination using the log-likelihood ratio based on spectral slope and ln(kurtosis) was also outlined.

Many interesting ocean areas have not been sampled, leaving unknown the levels and distribution of small-scale activity in those regions. Scientists are endeavoring to tie observations of microstructure to larger-scale processes, but success in identifying the particular physical mechanism producing the microstructure is still limited. A great deal of work is left to be done.

REFERENCES

[1] Schmitt, R. W., "Form of the Temperature–Salinity Relationship in the Central Water: Evidence for Double-Diffusive Mixing," *J. Phys. Oceanogr.* **11**, 1015–1026 (1981).

[2] Hamilton J. M., Lewis, M. R., and Ruddick, B. R., "Vertical Fluxes of Nitrate Associated with Salt Fingers in the World's Oceans," *J. Geophys. Res.* **94**, 2137–2145 (1989).

[3] Schmitt, R. W., "Overview of C-Salt," in *Double Diffusion in Oceanography: Proc. Meeting September 26–29, 1989*, WHOI-91-20, Woods Hole Oceanographic Institution, pp. 11–30 (1991).

[4] Shay, T. J., and Gregg, M. C., "Convectively Driven Turbulent Mixing in the Upper Ocean," *J. Phys. Oceanogr.* **16**, 1777–1798 (1986).

[5] Thorpe, S. A., "Experiments on the Instability of Stratified Shear Flows: Miscible Fluids, *J. Fluid Mech.* **46**, 299–319 (1971).

[6] Miles, J. W., "On the Stability of Heterogeneous Shear Flows," *J. Fluid Mech.* **10**, 496–508 (1963).

[7] Gregg, M. C., D'Asaro, E., Shay, T. J., and Larson, N., "Observations of Persistent Mixing and Near-Inertial Internal Waves," *J. Phys. Oceanogr.* **16**, 856–885 (1986).

[8] Turner, J. S., *Buoyancy Effects in Fluids*, Cambridge University Press, Cambridge, England (1973).

[9] Gargett, A. E., and Schmitt, R. W., "Observations of Salt Fingers in the Central Waters of the Eastern North Pacific," *J. Geophys. Res.* **87**, 8017–8029 (1982).

[10] Brandt, A., and Hurdis, D. A., "Simulation of Oceanographic Processes in the Hydrodynamics Research Laboratory," *Johns Hopkins APL Tech. Dig.* **3**, 42–48 (1982).

[11] Mack, S. A., and Schoeberlein, H. C., "Discriminating Salt-Fingering from Turbulent Induced Microstructure in Towed Conductivity Array Data," in *Double Diffusion in Oceanography: Proc. Meeting September 26–29, 1989*, WHOI-91-20, Woods Hole Oceanographic Institution pp. 103–114 (1991).

[12] Baker, M. A., and Gibson, C. H., "Sampling Turbulence in the Stratified Ocean: Statistical Consequences of Strong Intermittency," *J. Phys. Oceanogr.* **17**, 1817–1836 (1987).

[13] Monin, A. S., and Yaglom, A. M., *Statistical Fluid Mechanics II, Vol. 2*, (English translation), The MIT Press, Cambridge, Mass. (1975).

[14] Kolmogorov, A. N., "A Refinement of Previous Hypotheses Concerning the Local Structure of Turbulence in a Viscous Incompressible Fluid at High Reynolds Number," *J. Fluid Mech.* **13**, 82–85 (1962).

[15] Gibson, C. H., "Kolmogorov Similarity Hypothesis for Scalar Fields: Sampling Intermittent Turbulent Mixing in the Ocean and Galaxy," in *Turbulence and Stochastic Processes: Kolmogorov's Ideas 50 Years On, Proc. R. Soc. Lond., Ser. A* **433**, 149–164 (1991) .

[16] Schoeberlein, H. C., "A Statistical Analysis of Patches of Oceanic Small-Scale Activity," *Johns Hopkins APL Tech. Dig.* **6**, 194–202 (1985).

[17] Holloway, G., and Gargett, A. E., "The Inference of Salt-Fingering from Towed Microstructure Observations," *J. Geophys. Res.* **92**, 1963–1965 (1987).

[18] Schmitt, R. W., and Evans, D. L., "An Estimate of the Vertical Mixing Due to Salt Fingers Based on Observations in the North Atlantic Central Waters," *J. Geophys. Res.* **83**, 2913–2919 (1978).

[19] Schmitt, R. W., "The Growth Rate of Super-Critical Salt Fingers," *Deep Sea Res.* **26A**, 23–40 (1979).

[20] Mack, S. A., "Two-Dimensional Measurements of Ocean Microstructure: The Role of Double Diffusion," *J. Phys. Oceanogr.* **15**, 1581–1604 (1985).

[21] Mack, S. A., "Towed-Chain Measurements of Ocean Microstructure," *J. Phys. Oceanogr.* **19**, 1108–1129 (1989).

[22] Marmorino, G. O., and Greenwalt, D., "Inferring the Nature of Microstructure Signals," *J. Geophys. Res.* **93**, 1219–1225 (1988).

[23] Marmorino, G. O., "Observations of Small-Scale Mixing Processes in the Seasonal Thermocline. Part I: Salt-Fingering," *J. Phys. Oceanogr.* **17**, 1339–1347 (1987).

[24] Batchelor, G. K., "Small-Scale Variation of Convected Quantities Like Temperature in Turbulent Fluid," *J. Fluid Mech.* **5**, 113–133 (1959).

[25] Gibson, C. H., and Schwarz, W. H., "The Universal Spectra of Turbulent Velocity and Scalar Fields," *J. Fluid Mech.* **16**, 365–384 (1963).

[26] Dillon, T. M., and Caldwell, D. R., "The Batchelor Spectrum and Dissipation in the Upper Ocean," *J. Geophys. Res.* **85**, 1910–1916 (1980).

[27] Oakey, N. S., Determination of the Rate of Dissipation of Turbulent Energy from Simultaneous Temperature and Velocity Shear Microstructure Measurements," *J. Phys. Oceanogr.* **12**, 256–271 (1982).

[28] Whalen, A.D., *Detection of Signals in Noise*, Academic Press, New York (1971).

[29] Kendall, M. G., and Stuart, A., *The Advanced Theory of Statistics, Vol. 2*, Hafner, Riverside, N.J. (1967).

ACKNOWLEDGMENTS: Peter Fuechsel provided valuable review comments. Mel Hennessy provided valuable software development and data processing assistance. This work has been supported in part by the Office of Naval Research under Contract N00039-91-C-0001 and by a Stuart S. Janney Fellowship.

THE AUTHORS

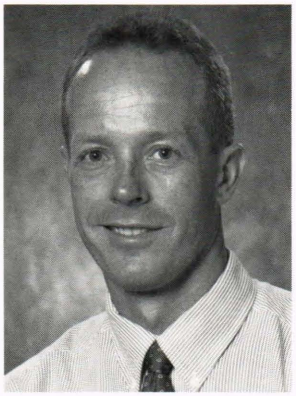

MARK A. BAKER received his Ph.D. in oceanography from the Scripps Institution of Oceanography, University of California, San Diego, in 1985. He joined APL in 1985 and is a member of the Principal Professional Staff and the Submarine Technology Department's Hydrodynamics Group (STH). Dr. Baker's main research interests are the statistics of small-scale mixing in the ocean and experiments on turbulent flow fields in the laboratory. Dr. Baker is the Supervisor of the STH Hydrodynamics Research and Calibration Laboratories. In October 1990, he participated in an oceanographic study aboard a Soviet research vessel on the influence of islands on the equatorial undercurrent in the western Pacific. He is a member of the American Meteorological Society, American Geophysical Union, Oceanography Society, IEEE Oceanic Engineering Society, Pi Mu Epsilon, and Sigma Pi Sigma.

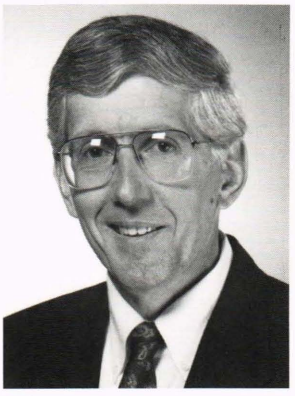

STEPHEN A. MACK received a B.S. degree in physics from St. Francis College in 1965, and M.S. and Ph.D. degrees (1967, 1971) in physics from Lehigh University. He was a postdoctoral fellow from 1971 to 1973 at the Department of Physics and Materials Research Department of the University of Illinois. Dr. Mack joined APL in 1973 and currently works in the Submarine Technology Department. He is interested in research on ocean small-scale mixing processes and has used both vertical profiling instruments and towed chain instruments to examine the relationship between ocean mixing and larger-scale ocean processes. He is a member of the Principal Professional Staff and Section Supervisor of the Applied Sciences Section of the Hydrodynamics Group. Dr. Mack has served on several Navy committees concerning oceanographic issues related to Navy needs.

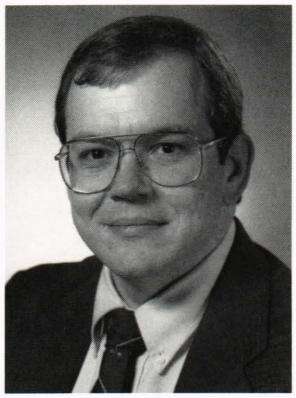

HOWARD C. SCHOEBERLEIN is a physicist with the APL Hydrodynamics Group. He obtained a B.S. in physics from Towson State University in 1975, followed by an M.S. in physics from Drexel University in 1977 and an M.S.E.E. from The Johns Hopkins University in 1984. After a two-year teaching assistantship at Drexel, Mr. Schoeberlein joined APL in 1977 as an associate physicist. His professional interests include digital signal processing, time series analysis, probability, and stochastic processes, with particular emphasis on applying these techniques to the analysis of small-scale oceanographic data. He is a member of Sigma Pi Sigma, the national physics honor society. He is a member of the Principal Professional Staff and Assistant Section Supervisor of the Measurement Physics Section of the Hydrodynamics Group.